Lawrence Berkeley National Laboratory
LBL Publications

Title
Efficient Fresnel zoneplate pattern data preparation for high-resolution nanofabrication

Permalink
https://escholarship.org/uc/item/0vb7f27b

Authors
Wang, Yow-Gwo
Miyakawa, Ryan H
Chao, Weilun
et al.

Publication Date
2017-11-01

DOI
10.1016/j.optcom.2017.05.060

Peer reviewed

eScholarship.org Powered by the California Digital Library
University of California

Efficient Fresnel Zoneplate Pattern Data Preparation for High-Resolution Nanofabrication

Yow-Gwo Wang,[a,b,*] Ryan H. Miyakawa,[b] Weilun Chao,[b] Patrick P. Naulleau[b]
[a]University of California, Berkeley, Department of Electrical Engineering and Computer Sciences, Berkeley, California, United States, 94720
[b]Lawrence Berkeley National Laboratory, Center for X-ray Optics, 1 Cyclotron Road, Berkeley, California, United States, 94720

Abstract. A Fresnel zoneplate is a diffractive optical element consisting of concentric rings (zones) for which the transmitted light produces a focal spot that is used in all wavelength regimes, including x-rays. The pattern of transmission openings determines the location of the spot and the sub-half wavelength size of the openings can adjust the intensity. Today, very general transmission zoneplate patterns are used for many special imaging and image compensation purposes. Manufacturing zoneplates require a zoneplate pattern file, which precisely describes the size, shape, and contour of the rings based on the desired optical properties of the lens. Generating such a pattern requires the delicate balance of achieving the required optical performance while maintaining manageable file sizes and computation times. Here we describe a new algorithm meeting these needs. By precisely controlling the number of shapes in each zone, the algorithm simultaneously optimizes the desired optical tolerances with the pattern file size.

Keywords: Fresnel zoneplate, Zoneplate pattern data preparation, X-ray, extreme ultraviolet (EUV).

***First Author, E-mail: henrywyg@berkeley.edu**

1 Introduction

The Fresnel zoneplate is an imaging element widely used by the x-ray and extreme ultraviolet (EUV) communities. In the soft x-ray regime, Fresnel zoneplates enable the possibilities for biological imaging and material science study into sub-10 nm regime [1]. In the past, papers regarding high-resolution zoneplates have mostly focused on optimizing the fabrication process conditions, rarely mentioned the detail of their pattern data preparation algorithm [2,3,4]. In this paper, we focus on the zoneplate pattern generation algorithm which can generate the desired zoneplate pattern and properly render it to a pattern file based on designed optical properties [5]. Figure 1 shows the general process flow of our algorithm. In the first section, we describe the generation of the target zoneplate pattern under various settings. Next, we discuss fracturing the

zoneplate pattern to meet fabrication requirement and optimize its file size and computation time. Finally, we present a few fabrication examples using the new algorithm.

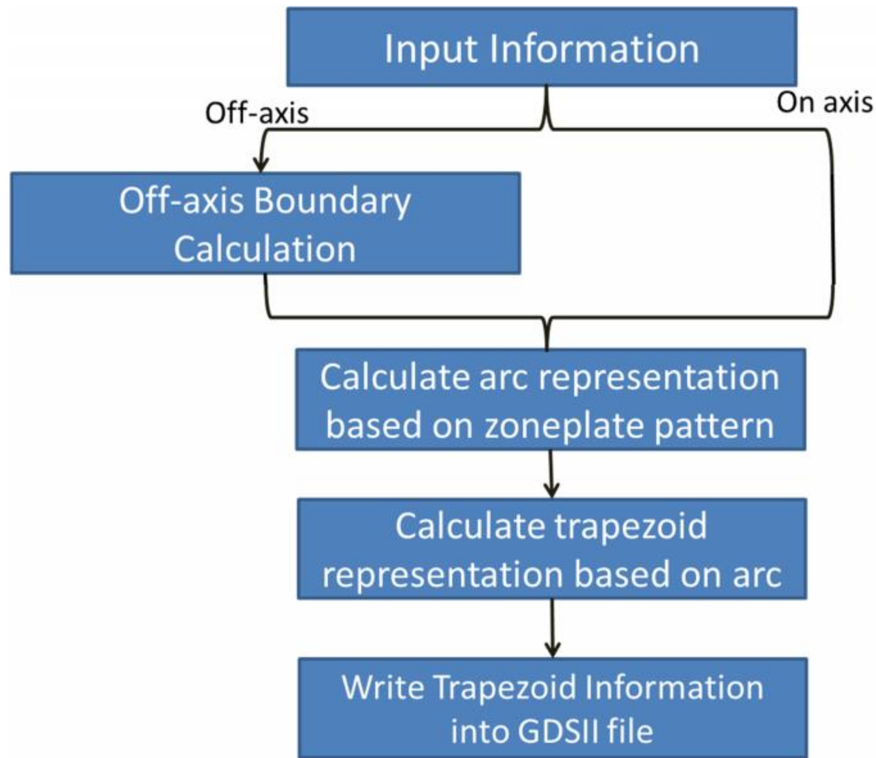

Fig. 1 The overall process flow of the zoneplate pattern generation algorithm

2 Fresnel zoneplate pattern generation algorithm

2.1 Zoneplate radii calculation algorithm

To calculate the zoneplate pattern, we need to define the zone radius at every point on the zoneplate to determine its contour. Figure 2 shows the process flow to determine the zone radius based on zone number (n), object distance (p), image distance (q), wavelength ( ), and also the aberration/phase contrast condition using the Secant method. In numerical analysis, the secant method is finite difference approximation of Newton's method for finding the zero crossing of a function.

Since the function used in the zoneplate is the optical path difference (OPD) for the complete optical system, an initial guess is needed for the Secant method to determine the correct zone radius. For our algorithm, we start with the assumption in the simple idea circular zoneplate lens as shown in Fig. 2. With this initial guess, the non-ideal OPD for the combination of geometry, aberration, and phase contrast is used to define a difference metric. The secant sequential iteration method is then used to sequentially find new roots (zero estimates) for this metric that converges to the spatial location on the zoneplate where the metric is zero.

$$Metric = (OPD_{geometry} + OPD_{aberration} + OPD_{phase_contrast}) - OPD_{zoneplate}, \quad (1)$$

This algorithm enables the possibility to (1) include arbitrary aberrations in the pattern calculation, and to (2) determine the balance between precision in locating the zone and computation time.

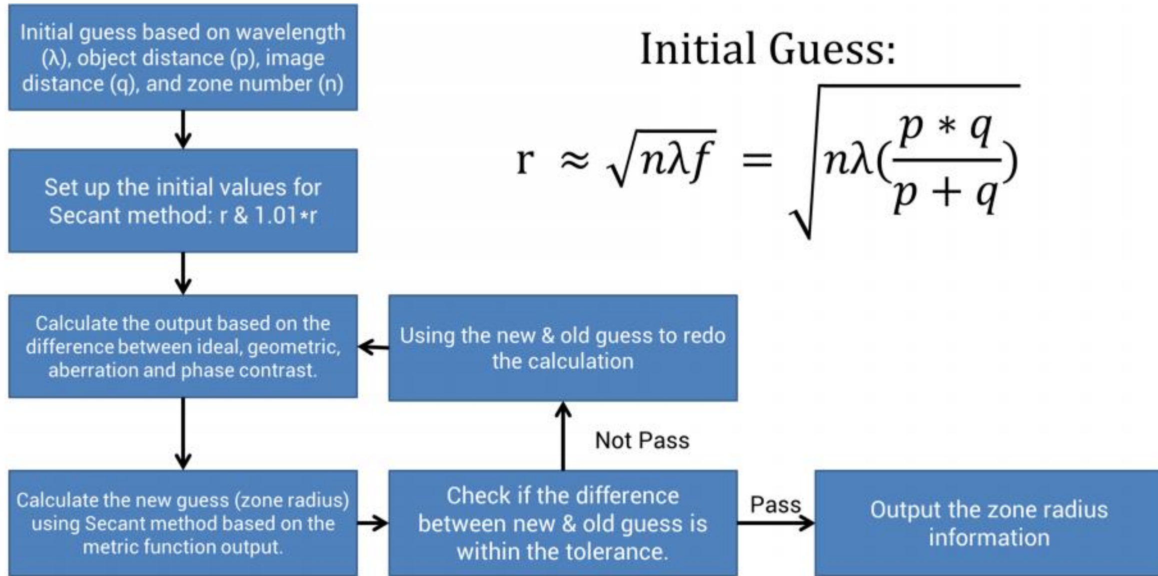

Fig. 2 The process flow of the algorithm on how to decide the zone radius using Secant method based on the OPD from geometric, phase contrast, and aberration.

2.2 On-axis / off-axis zoneplate

The process flow to determine a conventional on-axis zoneplate pattern is shown in Fig. 3. With design information like object distance, image distance, the numerical aperture (NA) and the wavelength, one can calculate the location, the width and the total number of the zones based on the equations shown in the previous section.

Off-axis zoneplates are useful for separating the zero order from the image forming orders and are used for the EUV mask reflection microscopy at Lawrence Berkeley National Laboratory [6]. In our algorithm, there is an extra step for the off-axis zoneplate compared to the on-axis zoneplate as shown in Fig. 3. The algorithm first calculates the opening angle for each zone based on the user-defined boundary condition and then generates the zoneplate pattern as done for the conventional on-axis zoneplate. Figure 4 shows the GDSII pattern image of an off-axis zoneplate on top of its parent on-axis zoneplate.

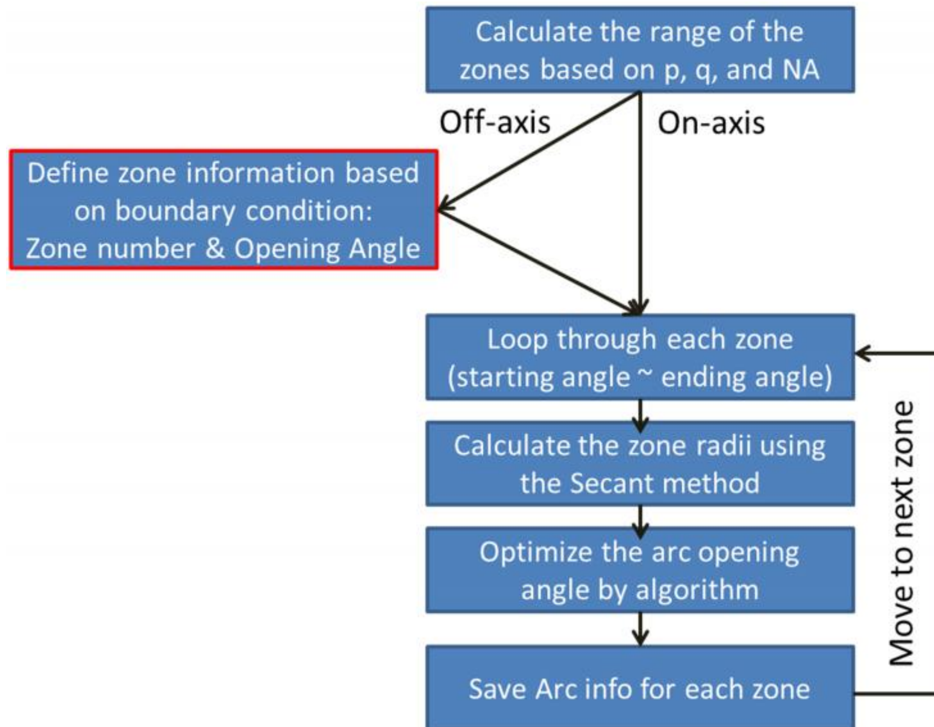

Fig. 3 The process flow of the algorithm on how to generate on-axis or off-axis zoneplate pattern.

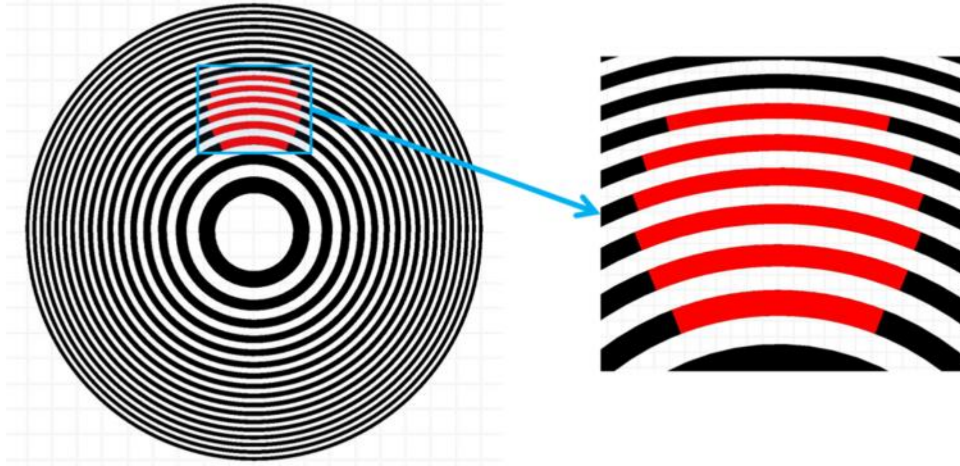

Fig. 4 GDSII pattern images of an off-axis zoneplate (red) on top of its parent on-axis zoneplate (black). The zoom-in view is shown on the right-hand side.

2.3 Tilted zoneplate

For tilted zoneplates, the zoneplate orientation is no longer normal to the optical axis, but each zone on the zoneplate still has to image the object to the same image plane position. Equation 2 shows the OPD calculation for a standard zoneplate:

$$OPD = (\sqrt{p^2 + r^2} - p) + (\sqrt{q^2 + r^2} - q)\,, \qquad (2)$$

Here p, q, r represent the object distance, the image distance and the zone radius before tilt. For tilted zoneplates, these parameters have to be adjusted accordingly. Figure 5a shows the schematic diagram of a tilted zoneplate and the adjustment required to Eq. 2. The tilted zoneplate which has the imaging capability based on p and q will be stretched on each side of the zoneplate as shown in Fig. 5b. In order to incorporate the tilted zoneplate situation into the pattern generation code, our algorithm adjusts the OPD definition as shown in Fig. 5a in the same process flow as for conventional on-axis zoneplate.

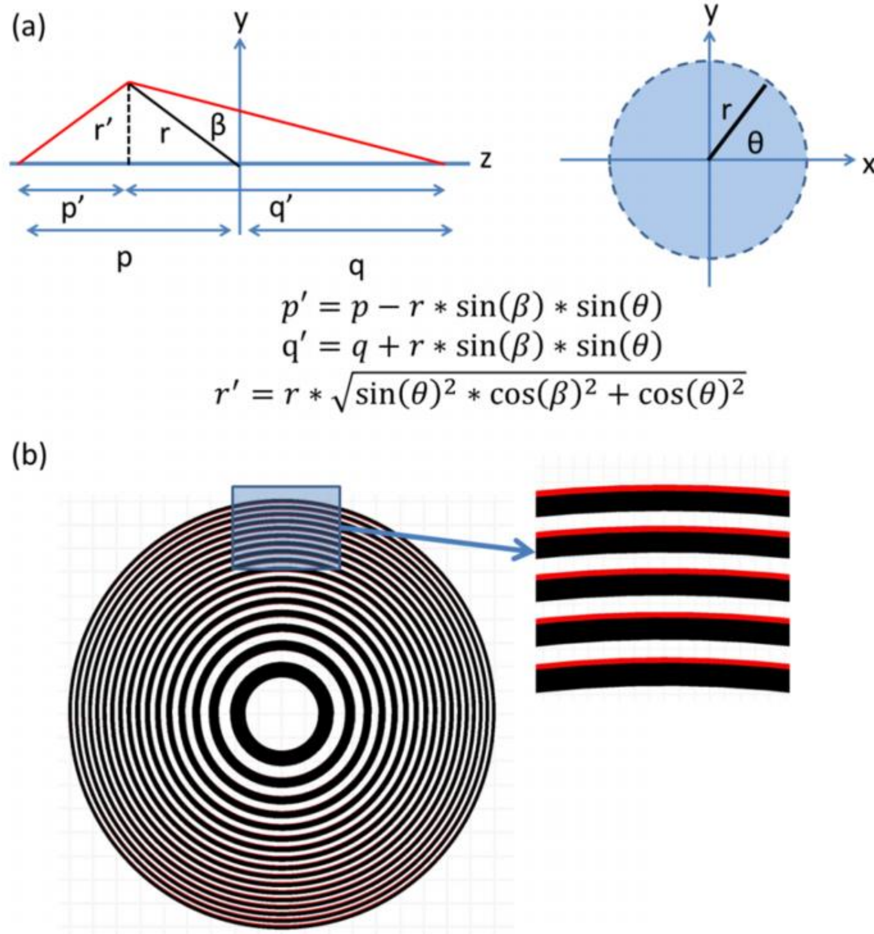

Fig. 5 (a) Schematic diagram of the definition of p', q', and r' based on the original p, q, and r, and also the tilt angle ( ) and its relative angle ( ) towards x-axis. (b) GDSII pattern images of a tilted on-axis zoneplate (red) on top of its parent standard zoneplate (black). The zoom-in view is shown on the right-hand side to show the shift of the zone when you tilt the zoneplate.

2.4 Phase contrast / aberration zoneplate

In general, the zone position is determined by the OPD including the geometric terms, aberration and phase contrast as shown in Eq. 3:

$$OPD = Geometric + Aberration + Phase_Contrsat\ , \qquad (3)$$

Zernike phase contrast is readily achieved in zoneplates by shifting the zones in the Zernike phase shift region to achieve a 90° relative phase shift. As shown in Eq. 1, the OPD for a standard zoneplate is in the range of half wavelength which can be transferred to 180° phase shifts. For phase contrast zoneplate with 90° phase shifts, our algorithm has to include quarter

wavelength into the OPD calculation to account for the phase difference. As shown in Fig. 6a, the shifts of the zone from its original position create the relative phase shifts between these 2 areas.

A similar approach can be applied to aberrations. Each point on the zoneplate has its own relative phase shift based on the input aberration condition. Thus the algorithm adjusts the OPD calculation accordingly to satisfy the condition at each location. For the pattern generation algorithm, the input aberration map consists of a Zernike polynomial representation [7]. Thus it can be used to prescribe not only the single aberration term onto the Fresnel zoneplate, but also more realistic aberration situations. Figure 6b shows the result of defocus aberration with a weight of half wavelength.

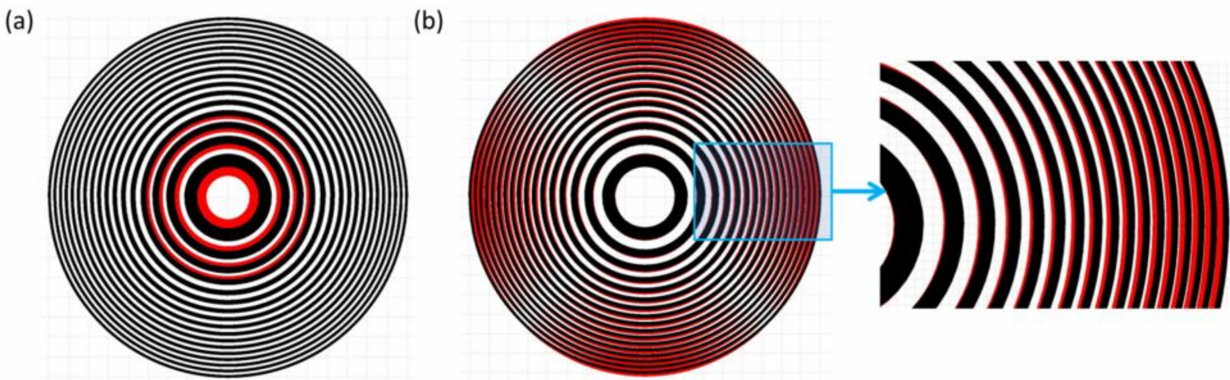

Fig. 6 (a) GDSII pattern images of a phase contrast zoneplate with 90° (quarter wavelength) phase shift in the central area of an on-axis zoneplate (red) on top of a standard zoneplate (black). (b) GDSII pattern images of an on-axis zoneplate with astigmatism aberration (red) on top of a standard zoneplate (black). Weight: 0.5 wavelength. The zoom-in view is shown on the right-hand side to show the shift of the zone when you prescribe the aberration onto the zoneplate.

2.5 Apodization / free-standing zoneplate

Apodization is used to filter or modify the transmission function of optical elements [8,9]. In order to achieve this in the algorithm, we add blocks to the ring-shaped zoneplate to prevent the light from passing through the zoneplate, instead of varying the zone width (duty cycle) which might be limited by the fabrication capability. Based on the designed transmission condition in

each zone, we can calculate the percentage of the zone area that needs to be blocked, and then randomly (but with uniform density) distribute the blocks to each zone as shown in Fig. 7a. Stronger apodization means lower transmission which leads to more blocks in each zone. For a constant apodization to be applied to a specific area of the zoneplate, blocks are randomly (but with uniform density) distributed in each zone. Figure 7a shows the comparison between a standard zoneplate and a zoneplate with constant apodization.

To improve zoneplate efficiency, zoneplates can be fabricated as free-standing structures instead of onto a membrane. In order to support the arc-shaped zoneplate structure, bridges are required as shown in Fig. 7b to hold the structure together. In the algorithm, the addition of these bridges is similar to the apodization process. Moreover, the algorithm supports the random distribution of the bridges preventing the unexpected frequency filtering by the Fresnel zoneplate.

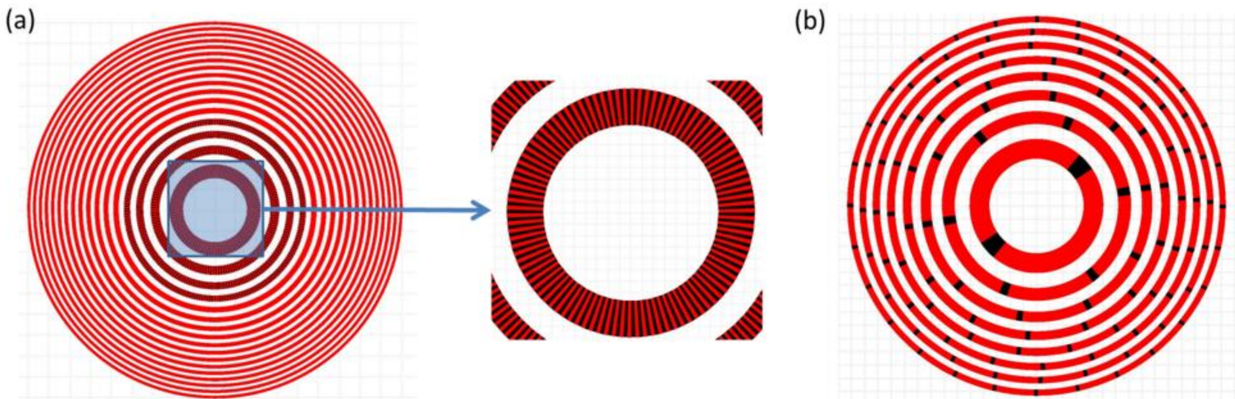

Fig. 7 (a) GDSII pattern images of an on-axis zoneplate with constant apodization aberration (red) in the central region on top of a standard zoneplate (black). The zoom-in view is shown at the right-hand side of the figure. (b) GDSII pattern images of a free-standing zoneplate (red) on top of a standard on-axis zoneplate (black). The random distribution of the bridges of the free-standing zoneplate can avoid unnecessary frequency filtering.

3 Fresnel zoneplate pattern rendering algorithm

3.1 Arc-shaped representation of the zoneplate pattern

Having a desired Fresnel zoneplate pattern, the design must be transferred into a file that can be read by lithography tools to fabricate the zoneplate. In order to achieve this, we need to find a proper representation of the zoneplate design using arcs or polygons. Therefore, an algorithm to render the zoneplate pattern is needed to balance the trade-off between file size (computation time) and precision of the polygons/arcs representation.

Figure 8 shows the process flow of fracturing the zoneplate pattern with arcs and the definition of the arc parameters for the zoneplate pattern representation. We start with an initial opening angle for the pattern. Then we use 3 sets of coordinates from this zone pattern to define the arc. Along the contour of the zone pattern and the arc, we compare the coordinate difference between them and check it within the user-defined tolerance. If it is within the range, the algorithm extends the opening angle to seek the opportunity using this arc to represent a larger zoneplate pattern. If not, then a smaller opening angle is used to check the condition again. This helps us minimize the number of arcs to represent the zoneplate pattern. With this algorithm, conventional zoneplates with a perfect circular shape can be represented by 1 arc (opening angle = 360°) as expected. Other zoneplates with exotic design will have its optimum number of arcs.

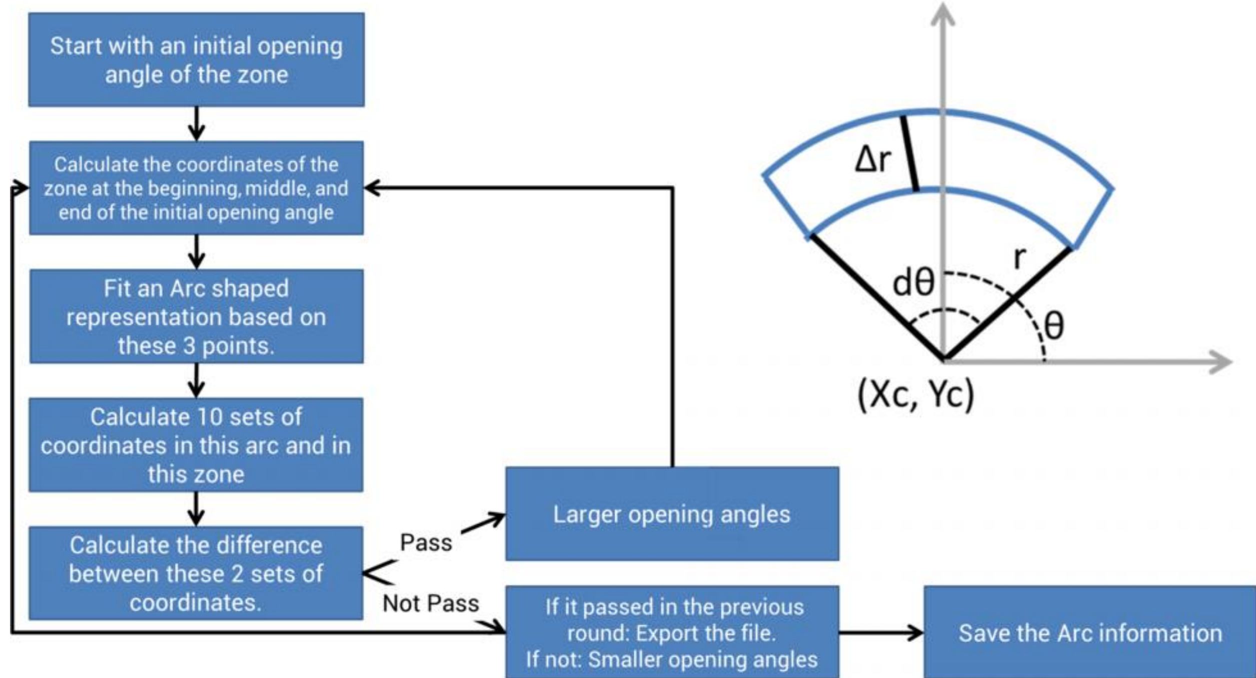

Fig. 8 The process flow of the algorithm on how to decide the arc representation of the zoneplate pattern. The insert figure shows the definition of arc parameters for zoneplate pattern representation. (Xc, Yc, r, r, , d) represents the center coordinates of the arc, arc radius, arc width, the starting angle of the arc, and the opening angle of the arc.

3.2 Trapezoid representation of the zoneplate pattern

Even though arc representation is really useful for curved Fresnel zoneplate pattern, we need trapezoid representation which is commonly required by most lithography tools. Figure 9a shows the process flow on how to transfer the zoneplate pattern representation using arcs to trapezoids.

The most critical factor for this process is the determination of how many trapezoids are needed to represent the arc properly. As shown on the right-hand side of Fig. 9b, we use the difference between the edge of the arc and trapezoid as the metric, normalized to the arc (zone) width. This tolerance definition keeps the error at every zone about the same amount in the unit of wavelength. The constant phase shift among every zone can reduce the potential to introduce unexpected aberration into the Fresnel zoneplate. Moreover, this variable allows the user to

determine the trade-off between file size (number of trapezoids) and the error tolerance on their zoneplate pattern design.

Figure 10 shows the impact of selected precision on file size for three different zoneplate sizes (number of zones). For a zoneplate with 1000 zones in it, the file size is within the range of 302 Mb to 3 Mb for a precision from 0.005% to 50%. For a zoneplate with 3000 zones in it, the file size range increases to 1558 Mb to 15 Mb for a precision from 0.005% to 50%. Generally, the file size increases linearly with the zone number, and it is inversely proportional to the precision.

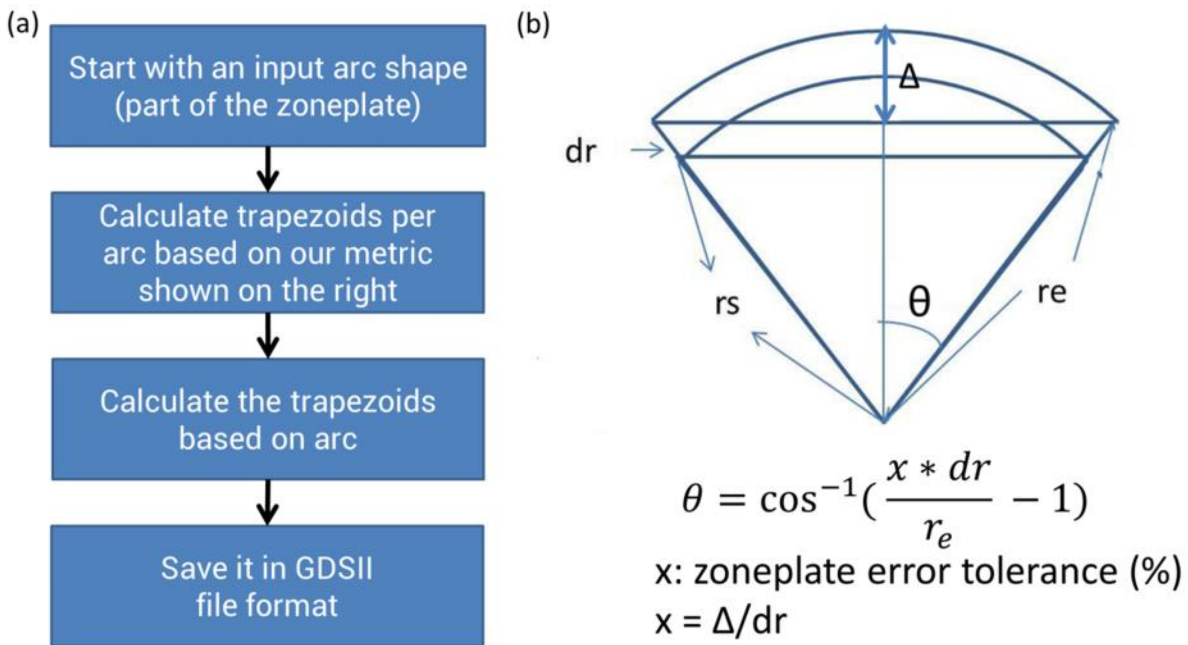

Fig. 9 (a) The process flow of the algorithm on how to render the arc into trapezoids for zoneplate pattern. (b) The metric used in the algorithm to determine the size of each trapezoid based on the user-defined tolerance.

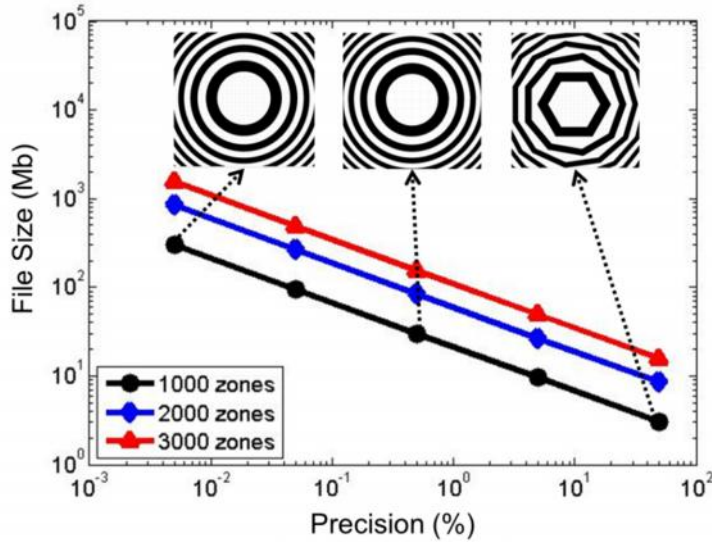

Fig. 10 The trade-off between GDSII file size and zoneplate pattern precision under different number of zoneplates: 1000 zones (Black), 2000 zones (Blue), 3000 zones (Red). The figure is in log-log scale. The insert figures show the center of the zoneplate pattern under different precision settings.

4 Fresnel zoneplate pattern fabrication demonstration

By using the algorithm described above, we generated trapezoid-rendered GDSII files of off-axis conventional and Zernike phase contrast zoneplate patterns based on the specific boundary conditions for the mask imaging EUV microscope [6] at Lawrence Berkeley National Laboratory. With the GDSII files, the patterns were fractured using internally developed code and were exposed on a Vistec VB300 electron-beam lithography system at the Molecular Foundry facility at Lawrence Berkeley National Laboratory. Figure 11 shows images of some of the fabricated zoneplates. Figure 11a is a conventional zoneplate and Figs.11b and 11c are Zernike phase contrast zoneplates.

The central circle area in Fig. 11b is phase-shifted. The zoom-in views in Fig. 11c show the displacement between the patterns to introduce the 90° phase shifts as well as the apodization produced by adding blocks to the desired area on the zoneplate to control the amount of light

passing through each zone. The phase shift and intensity transmission are indicated in the figure for each zoneplate.

Imaging performance of the microscope using the conventional zoneplate is described in Ref. [10] and effectiveness of the Zernike phase contrast zoneplates in enhancing the detection of sub-nm EUV multilayer defects is described in Refs. [11] and [12]. Comparing the measured contrast transfer function results presented in Ref. [10] to the simulation results for an ideal diffraction limited system (Fig. 12), we find the patterned zoneplate to be operating at the diffraction limit.

In addition to working for systems where the zoneplate is orthogonal to the chief ray, our algorithm also supports tilted zoneplates to deal with the tilted geometry systems often useful for reflection imaging [13]. Figure 13 shows an example of such a zoneplate designed to work with the chief ray at 6° relative to the zoneplate surface normal. Although not obvious from the image, this results in a slightly elliptical zoneplate. The zoneplate in Fig. 13 is designed to work at a wavelength of 13.56 nm, has a numerical aperture of 0.0875, and a diameter of approximately 100 um.

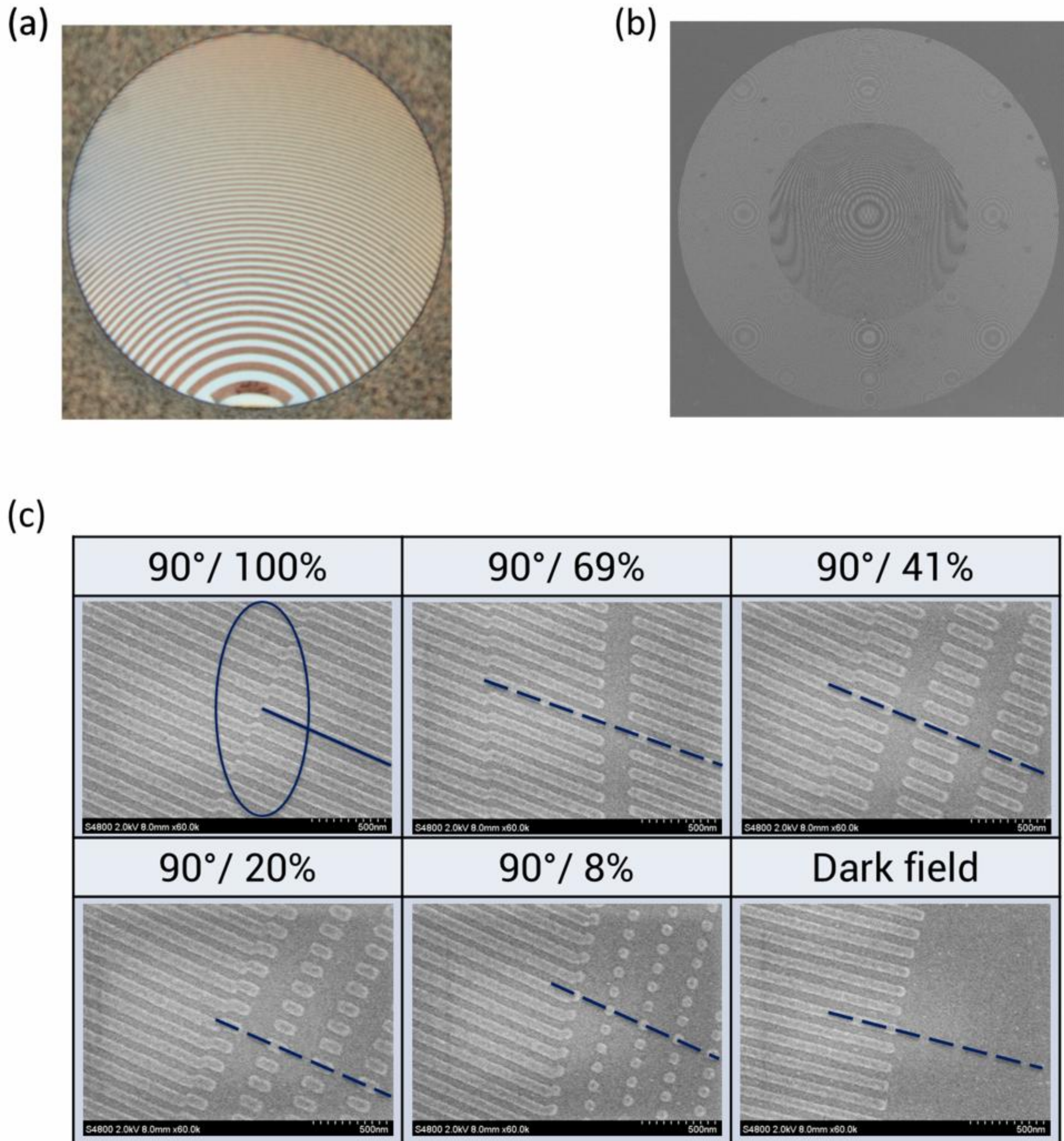

Fig. 11 (a) Optical image of a standard off-axis zoneplate used by the mask imaging EUV microscope at Lawrence National Berkeley Laboratory. The diameter of the zoneplate is approximately 100 um. (b) SEM image of an off-axis zoneplate with phase contrast and apodization in the central area. (c) The table shows zoom-in SEM images of the zoneplates with different apodization conditions to control the transmission as indicated in the table. Circle area shows the quarter wavelength displacement which creates the 90° phase shifts and the line indicated the area with reduced intensity transmission.

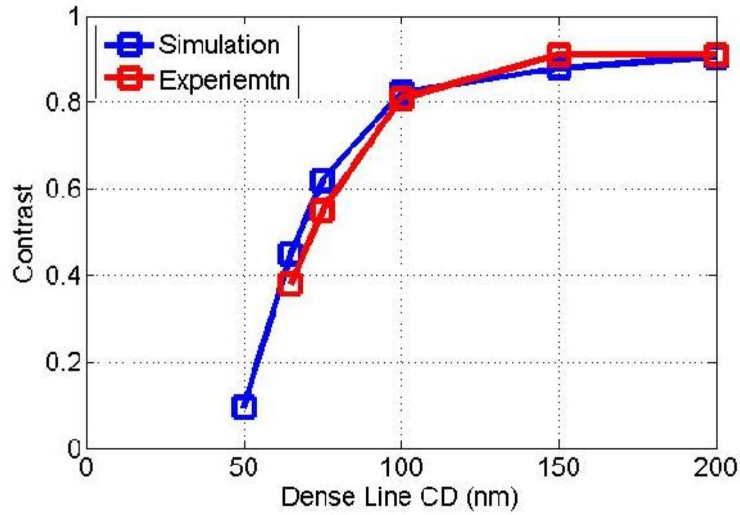

Fig. 12 Contrast vs. CD for dense lines. Simulation results (Blue), and experiment data (Red) from Ref. [10]. 4xNA = 0.33, partial-coherence = 0.8. 3.75% of flare is added into the simulation images.

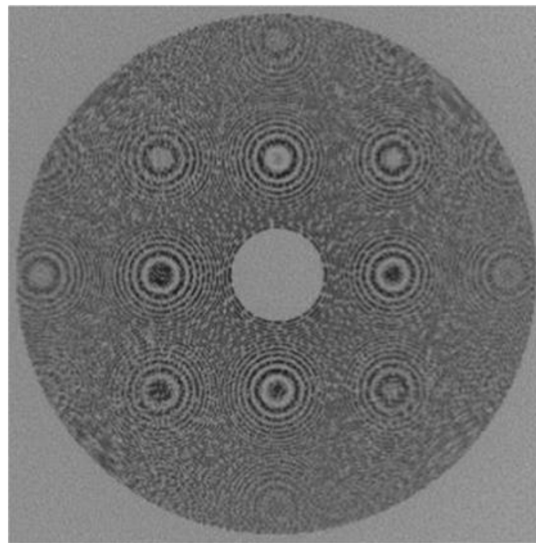

Fig. 13 SEM image of a tilted zoneplate used by the EUV scanning beam microscope [13].

5 Conclusion

In this paper, we described a new algorithm to generate fabrication-ready zoneplate patterns. The algorithm can generate both on and off-axis zoneplate patterns, as well as arbitrary phase/intensity modulation. Moreover, a user-defined tolerance setting in the fracturing algorithm keeps the flexibility in the computation time and the precision of the zoneplate pattern.

The algorithm has been used to generate Fresnel zoneplates used by the EUV mask microscope [6] at Lawrence Berkeley National Laboratory for standard imaging and other exotic imaging modes as well as tilted zoneplates for use in a scanning EUV microscope [13].

Acknowledgments

This work was performed in part at Lawrence Berkeley National Laboratory which is operated under the auspices of the Director, Office of Science, of the U.S. Department of Energy under Contract No. DE-AC02-05CH11231.

References

1. W. Chao, BD. Harteneck, JA. Liddle, EH. Anderson, and DT. Attwood, “Soft X-ray microscopy at a spatial resolution better than 15nm,” Nature 435, 1210-1213 (2005).
2. A. Ozawa, T. Tamamura, T. Ishii, H. Yoshihara, and T. Kagoshima, “Application of X-ray mask fabrication technologies to high resolution, larger diameter Ta Fresnel zoneplates,” Microelectron. Eng.35, 525 (1997).
3. S.J. Spector, C. J. Jacobsen, and D. M. Tennant, “Process optimization for production of sub-20 nm soft X-ray zoneplates,” J. Vac. Sci. Technol. B 15(6), 2872-2876 (1997).
4. Y. Feng, M. Feser, A. Lyon, S. Rishton, X. Zeng, S. Chen, S. Sassolini, and W. Yun, “Nanofabrication of high aspect ratio 24 nm X-ray zoneplates for X-ray imaging applications,” J. Vac. Sci. Technol. B 25(6), 2004-2007 (2007).
5. http://zoneplate.lbl.gov (2017).
6. K. Goldberg, I. Mochi, M. Benk, A. Allezy, M. Dickinson, C. Cork, D. Zehm, J. Macdougall, E. Anderson, F. Salmassi, W. Chao, V. K. Vytla, E. Gullikson, J. Deponte, M. S. Gideon Jones, D. Camp, J. Gamsby, W. Ghiorso, H. Huang, W. Cork, E. Martin, E. Every, E. Acome, V. Milanovic, R.

Delano, P. Naulleau, and S. Rekawa, “Commissioning an EUV mask microscope for lithography generations reaching 8 nm,” SPIE Proc. 8679, 867919 (2013).

7. S. N. Bezdidko, “The use of Zernike polynomials in optics,” Sov. J. Opt. Technol. 41, 425-429 (1974).
8. G. Schmahl, D. Rudolph, B. Niemann, and O. Christ, “Zone-plate X-ray microscopy,” Quarterly Reviews of Biophysics 13(3), 297-315 (1980).
9. W. H. Southwell, “Using apodization functions to reduce sidelobes in rugate filters,” Appl. Opt. 28(23), 5091-5094 (1989).
10. K. Goldberg, M. Benk, A. Wojdyla, D. Johnson, A. Donoghue, “New ways of looking at masks with the SHARP EUV microscope,” SPIE Proc. 9422, 94221A (2015).
11. Y.G. Wang, R. Miyakawa, A. Neureuther, P. Naulleau, “Zernike phase contrast microscope for EUV mask inspection”, SPIE Proc. 9048, 904810 (2014).
12. Y.G. Wang, R. Miyakawa, W. Chao, M. Benk, A. Wojdyla, A. Donoghue, D. Johnson, K. Goldberg, A. Neureuther, T. Liang, P. Naulleau, “Enhancing defect detection with Zernike phase contrast in EUV multilayer blank inspection,” SPIE Proc. 9422, 94221C (2015).
13. P. Naulleau, C. Anderson, E. Anderson, N. Anderson, W. Chao, C. Choi, K. Goldberg, E. Gullikson, S. S. Kim, D. Lee, R. Miyakawa, J. Park, S. Rekawa, F. Salmassi, “Electro-optical system for scanning microscopy of extreme ultraviolet masks with a high harmonic generation source,” Opt. Express 22(17), 20144-20154 (2014).

Yow-Gwo Wang is a Ph.D. candidate in Electrical Engineering and Computer Sciences at the University of California, Berkeley, and also a graduate student researcher at the Center for X-ray Optics, Lawrence Berkeley National Laboratory. His current research project is focused on design, fabrication and testing new concept for high sensitivity EUV aerial image inspection

under the guidance of Prof. Andrew Neureuther and Dr. Patrick Naulleau. He was the recipient of SPIE BACUS Scholarship in 2015.

Ryan H. Miyakawa is a research scientist at the Center for X-ray Optics at Lawrence Berkeley National Lab, where he works with the Berkeley MET performing EUV imaging, interferometry, and lithography.

Weilun Chao leads the nanofabrication group of the Center for X-ray Optics. He received his Ph.D. in electrical engineering from the University of California, Berkeley, in 2005. He specializes in electron-beam-based lithographic processes for dense nanostructures and EUV/x-ray diffractive optics. Current research interests include complex diffractive optics, 3-D nanostructures, and nanodevices for life science.

Patrick P. Naulleau received his BS and MS degrees in electrical engineering from Rochester Institute of Technology, Rochester, New York, and his Ph.D. in electrical engineering from the University of Michigan, Ann Arbor, in 1997. He joined the Berkeley Lab working in EUV lithography and metrology. In April 2010, he became director of the Center for X-ray Optics at the Berkeley Lab. He has over 300 publications and 19 patents and is a fellow of OSA and SPIE.

Caption List

Fig. 1 The overall process flow of the zoneplate pattern generation algorithm

Fig. 2 The process flow of the algorithm on how to decide the zone radius using Secant method based on the OPD from geometric, phase contrast, and aberration.

Fig. 3 The process flow of the algorithm on how to generate on-axis or off-axis zoneplate pattern.

Fig. 4 GDSII pattern images of an off-axis zoneplate (red) on top of its parent on-axis zoneplate (black). The zoom-in view is shown on the right-hand side.

Fig. 5 (a) Schematic diagram of the definition of p', q', and r' based on the original p, q, and r, and also the tilt angle ( ) and its relative angle ( ) towards x-axis. (b) GDSII pattern images of a tilted on-axis zoneplate (red) on top of its parent standard zoneplate (black). The zoom-in view is shown on the right-hand side to show the shift of the zone when you tilt the zoneplate.

Fig. 6 (a) GDSII pattern images of a phase contrast zoneplate with 90° (quarter wavelength) phase shift in the central area of an on-axis zoneplate (red) on top of a standard zoneplate (black). (b) GDSII pattern images of an on-axis zoneplate with astigmatism aberration (red) on top of a standard zoneplate (black). Weight: 0.5 wavelength. The zoom-in view is shown on the right-hand side to show the shift of the zone when you prescribe the aberration onto the zoneplate.

Fig. 7 (a) GDSII pattern images of an on-axis zoneplate with constant apodization aberration (red) in the central region on top of a standard zoneplate (black). The zoom-in view is shown at the right-hand side of the figure. (b) GDSII pattern images of a free-standing zoneplate (red) on top of a standard on-axis zoneplate (black). The random distribution of the bridges of the free-standing zoneplate can avoid unnecessary frequency filtering.

Fig. 8 The process flow of the algorithm on how to decide the arc representation of the zoneplate pattern. The insert figure shows the definition of arc parameters for zoneplate pattern representation. (Xc, Yc, r, r, , d) represents the center coordinates of the arc, arc radius, arc width, the starting angle of the arc, and the opening angle of the arc.

Fig. 9 (a) The process flow of the algorithm on how to render the arc into trapezoids for zoneplate pattern. (b) The metric used in the algorithm to determine the size of the trapezoid based on user-defined tolerance.

Fig. 10 The trade-off between GDSII file size and zoneplate pattern precision under different number of zoneplates: 1000 zones (Black), 2000 zones (Blue), 3000 zones (Red). The insert figure shows the center of the zoneplate pattern under different precision settings.

Fig. 11 (a) Optical image of a standard off-axis zoneplate used by the mask imaging EUV microscope at Lawrence National Berkeley Laboratory. The diameter of the zoneplate is approximately 100 um. (b) SEM image of an off-axis zoneplate with phase contrast and apodization in the central area. (c) The table shows zoom-in SEM images of the zoneplates with different apodization conditions to control the transmission as indicated in the table. Circle area shows the quarter wavelength displacement which creates the 90° phase shifts and the line indicated the area with reduced intensity transmission.

Fig. 12 Contrast vs. CD for dense lines. Simulation results (Blue), and experiment data (Red) from Ref. [10]. 4xNA = 0.33, partial-coherence = 0.8. 3.75% of flare is added into the simulation images.

Fig. 13 SEM image of a tilted zoneplate used by the EUV scanning beam microscope [13].